UNIVERSITY OF BIRMINGHAM

University of Birmingham Research at Birmingham

Hydrogen sorption properties of LixNa1−xMgH3 (x = 0, 0.2, 0.5 & 0.8)

Contreras Vasquez, Luis; Liu, Yinzhe; Paterakis, Christos; Reed, Daniel; Book, David

[Link to publication on Research at Birmingham portal](#)

Hydrogen Sorption properties of $Li_xNa_{1-x}MgH_3$ (x=0, 0.2, 0.5 & 0.8)

Luis. F. Contreras Vasquez[a,*], Yinzhe Liu[a], Christos Paterakis[a], Daniel Reed[a], David Book[a]

[a] School of Metallurgy and Materials, University of Birmingham, Edgbaston, Birmingham B15 2TT, UK

Abstract

The synthesis, thermodynamic destabilisation and hydrogen absorption/desorption characteristics of the $Li_xNa_{1-x}MgH_3$ system with (x=0, 0.2, 0.5 and 0.8 molar ratios) have been investigated. Samples were mechanically milled under argon for 5 hours; then characterised by X-ray diffraction (XRD), differential scanning calorimetry (DSC), and thermogravimetric analysis (TGA). Diffraction peaks of $NaMgH_3$ phase shifted to higher angles and lattice parameters decreased due to the Li addition into the system. 2 and 3 endothermic reactions were observed for the Li_x substituted samples (x=0, 0.2, 0.5, 0.8). $Li_{0.8}Na_{0.2}MgH_3$ hydride showed the best performance among the other quaternary hydrides (synthesised in this work) releasing 5.2 wt.% of H_2 at 314 °C. Rehydrogenation of the decomposed $Li_xNa_{1-x}MgH_3$ (x=0, 0.2, 0.5 & 0.8) samples was experimentally confirmed under 10 bar H_2 at ~250 °C.

1. Introduction

Hydrogen is a clean energy vector that has the potential to replace carbon–based fuels. However, due to a lack of efficient technologies for storage, its commercial application is still limited in mobile applications [6,15,26,27]. Solid-state hydrogen storage gives an attractive volumetric storage density, however, there is a need to identify reversible hydrides which are mostly composed of lighter elements. Ternary compounds with perovskite structure (ABH_3) where H is the anion and A monovalent (alkali or alkaline earth metal) and B divalent (transition metal) are cations have attracted attention; particularly, magnesium and alkali elements due to their light-weight and relative abundance [12,16,19].

Amongst the perovskite ternary hydrides, $NaMgH_3$ has stood out due to its relatively high theoretical volumetric and gravimetric hydrogen storage densities (88 kg/m^3 & 6 wt.%), and the ability to reversibly absorb and desorb H_2 [2,3,18]. In addition, due to its superior hydrogen mobility, this perovskite structure is a promising material for future electronic devices due to its high ionic conductivity[16]. $NaMgH_3$ has an orthorhombic crystal structure similar to the $GdFeO_3$ type (Pnma space group)[1]. The desorption enthalpy ΔH (86.6 ± 1.0 kJ/mol H_2) and entropy ΔS (132.2 ± 1.3 kJ/ mol H_2 K) have been reported by Sheppard et al., showing that $NaMgH_3$ presents a lower thermodynamic stability in comparison to MgH_2[20,21]. Nevertheless, dehydrogenation temperature of the ternary hydride at approximately 400 °C is higher than the US DOE target for on-board H_2 storage for light-duty vehicles[14]. Therefore, there is a need to enhance the sorption kinetics and lower the decomposition temperatures of the ternary $NaMgH_3$ hydride.

It has been shown that sorption kinetics can be accelerated by the addition of catalytic additives, whereas thermodynamic properties can be modified by the formation of new alloys [4,24]. For example, Chaudhary et. al.[4] reported lower onset decomposition temperatures after adding Si to NaMgH$_3$. Hui Wu et. al.[24] studied the crystal chemistry of NaMgH$_3$ and reported that the perovskite crystal structure might be employed to synthesise new alloys with improved hydrogen storage properties[16, 24].

Several techniques have been used for the synthesis of the ternary NaMgH$_3$ hydride. For instance, the reaction of the hydrides under high pressures[1], cryo-milling and high-pressure H$_2$ sintering[13,16,20], mechanochemical synthesis under H$_2$[8], and Ar atmospheres [17].Mechanochemical approaches are advantageous in comparison to other methods, because they reduce the grain size, hence accelerating the H$_2$ desorption kinetics of the hydrides[9,10, 22].

Furthermore, it has been established that replacing transition metal (B) with alkali/alkaline earth metal in the ABH$_3$ system can enhance gravimetric capacity when light metals (i.e. Li, Mg, Na) are incorporated [5, 7, 9-11, 17]. Ikeda et.al reported formation ability of Li$_x$Na$_{1-x}$MgH$_3$ (x=0, 0.5 & 1) after mechanical milling NaH, MgH$_2$ and LiH for 20 h under a hydrogen atmosphere. (x=0) composition resulted in a single phase NaMgH$_3$ compound, while for (x=0.5, 1) unreacted remains of MgH$_2$ was detected[10]. Xiao et al. performed density functional theory (DFT) calculations on Li$_x$Na$_{1-x}$ MgH$_3$, predicting that substituting Li for Na into the system will lead to a decrease in unit-cell parameters, due to the smaller ionic size of Li$^+$ (compared to Na$^+$)[25]. Martinez et.al., synthesised Na$_{1-x}$Li$_x$MgH$_3$ (x= 0, 0.25 & 0.5) employing high-pressure techniques[13] and Zhong-min and co-workers formed the quaternary Na$_{1-x}$Li$_x$MgH$_3$ hydride (x=0, 0.5, 1.0) by mechanical milling under H$_2$ atmosphere (0.8 MPa) for 45 hours[23]. Both studies experimentally confirmed Xiao's DFT predictions.

Moreover, rehydrogenation of perovskite-type NaMgH$_3$ has been reported under 10 bar of hydrogen at 400 °C, from the decomposed phase of Na and Mg[8]. However, no reports related to the re-hydrogenation properties of quaternary Li$_x$Na$_{1-x}$MgH$_3$ hydride were found and therefore, will need to be studied.

This paper describes the study of the synthesis, structural changes, thermal analysis and re-hydrogenation properties of a 5 hours milled under argon alone Li$_x$Na$_{1-x}$MgH$_3$ hydride with nominal compositions (x=0, 0.2, 0.5, 0.8), using a combination of experimental techniques (i.e. Ex-situ and In-Situ X-ray Diffraction, Differential Scanning Calorimetry, and Thermogravimetric Analysis); to the best of the authors' knowledge, synthesis of the hydride via mechanical milling under argon alone, has not been reported in previous investigations.

Experimental

Powders of MgH$_2$ (95% pure hydride phase and remainder 5% Mg; Sigma-Aldrich Inc.), NaH (95% pure; Sigma-Aldrich Inc.) and LiH (99.9% pure; Sigma-Aldrich Inc.) were mixed to obtain the following composition: Li$_x$Na$_{1-x}$MgH$_3$, (x= 0, 0.2, 0.5, and 0.8). Mixtures were placed in a 250 ml stainless steel vial with stainless steel balls diameter of 10 mm. The ball to sample mass ratio was 50:1. Samples were mechanically milled in a planetary ball mill apparatus (Retsch Planetary Ball Mill PM400) in 1 bar Ar for 10 hours (in total) at 400 rpm

with intervals of 5 min of milling followed by 5 minutes' rest time to prevent decomposition of the samples due to overheating during milling. As-prepared samples were characterised by Ex-Situ powder X-ray Diffraction (XRD) with a Bruker D8 Advance diffractometer using Cu Kα (0.154nm) radiation, controlled by Diffract software. Samples were loaded in a dome-shaped sample holder inside an argon-filled glove box and then transferred to the instrument for analysis. For the study of the structural changes, In-Situ X-ray diffraction (XRD) measurements were carried out using an Anton Paar XRK 900 reactor chamber. The patterns were collected from 30 to 430 °C in 3 bar Ar for dehydrogenation, and 10 bar H_2 for rehydrogenation. Samples were contained in a boron nitride sample holder, and a time of ~43 minutes was required to collect a diffraction pattern in the $5 \leq 2\theta(°) \leq 90$ range for phase determination. Ex/In-Situ diffractions were analysed using EVA software (equipped with PDF – 2 database).[28] Pseudo-Rietveld Refinement was performed using TOPAS Academic Software[29] with reference data obtained from the Inorganic Crystal Structure Database (ICSD). The background was modelled using a Chebyshev function. Peak shapes were fitted using the Pseudo-Voight function. The lattice parameters were adapted, following the atomic parameters. To obtain a more accurate fitting all points before 25 $2\theta(°)$ were excluded from the refinement.

Thermal analysis was carried out using a thermogravimetric system (Netzsch TG 209) working at a heating rate of 2 °C/min, under 40 ml/min flowing argon. Differential Scanning Calorimetry (DSC) analysis was performed using a (Netzsch DSC 204 HP Phoenix) in a temperature range of 25-430 °C. The heating rate was 2 °C/min, under 100 ml/min flowing argon at 3 bars constant pressure. All thermal analysis experiments were conducted inside and argon –filled glove box with purified argon of less than 5 ppm oxygen using alumina crucible covered with a lid.

3. Results and discussion

3.1 Formation and analysis of the perovskite-type system

Figure1 shows the XRD patterns of the ball milled $Li_xNa_{1-x}MgH_3$ (x= 0, 0.2, 0.5, & 0.8). After 5 hours milling for the x=0 composition, peaks of $NaMgH_3$ phase can be identified which correspond to the orthorhombic (space group Pnma) perovskite-type structure. There are also unreacted peaks corresponding to NaH and MgO phases, the last can be related to oxidation due to the milling process. With the Li substitution x=0.2, a slight decrease of peak intensity in the main $NaMgH_3$ phase is observed and the same unreacted NaH phase is present, LiH is not observed, presumably because it reacted with NaH and MgH_2 mixtures on milling, leading to a lattice contraction in the main $NaMgH_3$ phase represented by a shift to a higher diffraction angles due to the smaller size of the Li cations (inset of Fig. 1). In the case of $Li_{0.5}Na_{0.5}MgH_3$, in addition to the main $NaMgH_3$ and NaH peaks, a new phase is formed after 5 hours milling corresponding to MgH_2. In the $Li_{0.8}Na_{0.2}MgH_3$ sample, $NaMgH_3$ and NaH along with MgH_2 phases can be observed. Neither in the x=0.5 nor in the x=0.8 samples LiH is detected. However, as a result of the shift to higher diffraction angles of the main

NaMgH$_3$ phase (inset Fig.1), it is inferred that Li ions are incorporated into the crystal structure of the system as replaces Na[13]. Moreover, the NaMgH$_3$ phase of the 5 h milled mixtures with nominal compositions x = 0, 0.2, 0.5 and 0.8 show an intensity decrease as the amount of Li increases, whereas MgH$_2$ and NaH intensities increase. This effect suggests that substitution of Na by Li can be performed up to a certain point; in the case of this research it is experimentally determined to be x = 0.5, when we go beyond that amount (i.e. x = 0.8) the intensity of the main phase is substantially decreased and more intense peaks of unreacted phases can be observed.
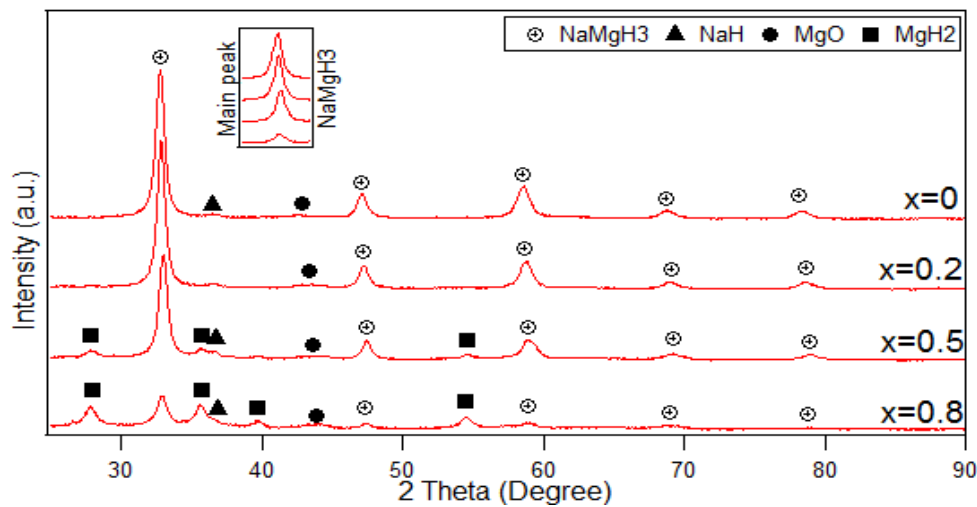

Figure 1 XRD patterns of 5h ball milled LixNa1-xMgH3 (x = 0, 0.2, 0.5, 0.8) hydride system. Main NaMgH3 peak zoomed in for the different Li x substitutions.

These events have been explained by Ikeda et. al. on the basis of the tolerance factor (t) calculations to predict the structure stability of ABX$_3$ perovskite-type hydrides. Ikeda et.al. reported that perovskite–type hydrides with stable structure are suggested to be within the range of tolerance factor (0.77 to 1.00)[8]. Therefore, in this investigation, Li$_x$Na$_{1-x}$MgH$_3$ substituted samples with nominal composition x = 0, 0.2 and 0.5 lay within this range showing a unit cell decrease tendency (Fig. 2), where it is evident that the sample containing Li$_x$ (x=0.8) substitution presents a different pattern, showing an increase in the cell volume since t value does not fall into the limit range.

In order to carry out a more accurate structural study, and to identify and quantify the phases of the Li$_x$Na$_{1-x}$MgH$_3$ (x= 0, 0.2, 0.5, & 0.8) hydride samples, Rietveld Refinement has been performed. (Appendix A) shows the refinement of the structural parameters of all active phases in the system. Results for the lattice parameters and cell volumes are contained in Table 1 and compared to previous literature reports.

Table 1   Lattice parameters for $Li_xNa_{1-x}MgH_3$ hydride (5h ball milled) compared to the literature data.

Lattice parameters $Li_xNa_{1-x}MgH_3$	This work				Martínez C. et al. [11]		
	x=0	x=0.2	x=0.5	x=0.8	x=0	x=0.25	x=0.5
a (Å)	5.484± 0.005	5.448± 0.007	5.451± 0.004	5.436± 0.134	5.46(6)	5.46(5)	5.46(1)
b (Å)	7.737± 0.007	7.688± 0.016	7.675± 0.006	7.689± 0.213	7.70(9)	7.70(8)	7.69(2)
c (Å)	5.425± 0.004	5.436± 0.011	5.393± 0.003	5.433± 0.126	5.41(6)	5.40(6)	5.39(1)
V (Å³)	230.487± 0.370	227.739± 0.744	225.656± 0.296	225.984± 0.240	227.88(4)	227.61(4)	226.96(9)

Lattice parameters obtained from the refinement significantly decrease as Li is added; Figure 2 presents the lattice parameters and cell volume of the 5 h milled $Li_xNa_{1-x}MgH_3$ samples in function of the Li substitution. It is evident from the plot that as more Li is substituted into the sample, the cell volume decreases; this reaction can be described by the smaller Li^+ ionic size with respect to the replaced Na^+ ions. Nevertheless, when the addition of Li reaches x=0.8 there is a significant increase in the cell volume.
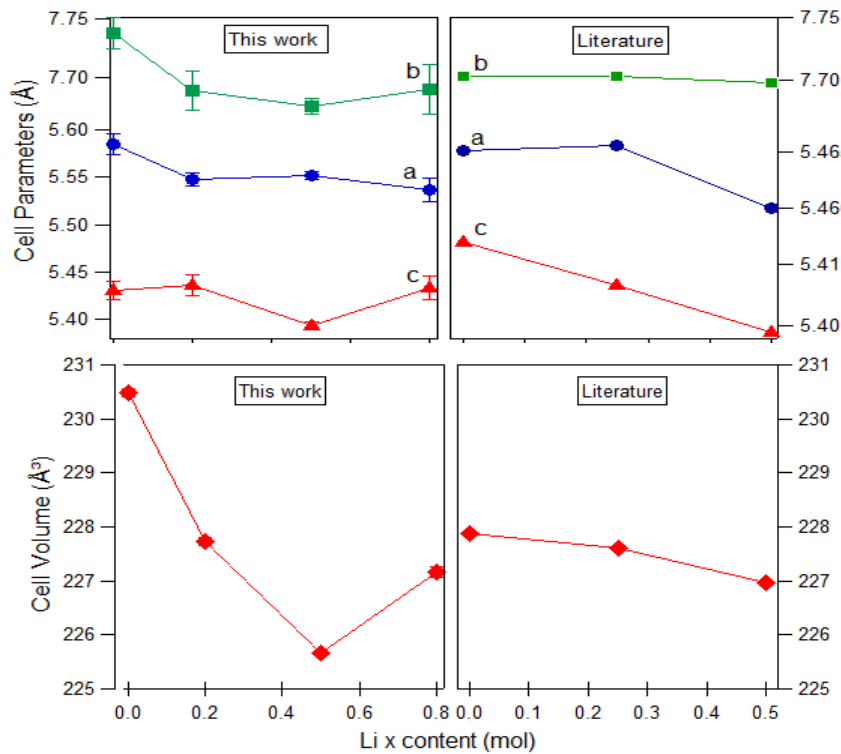

Fig. 2 Unit cell parameters (top) and Cell Volume parameters (bottom) of $Li_xNa_{1-x}MgH_3$ hydride system in function of Li substituted into the system. This work (left) vs literature (right)[11]. Where error bars are not shown they are smaller than the data symbols.

3.2 Measurement of hydrogen storage capacity

3.2.1 (Thermal analysis DSC, TGA, In-situ XRD)

Thermal analysis was conducted via DSC and TGA measurements in order to study the dehydriding mechanisms, thermal transitions and mass changes of the quaternary $Li_xNa_{1-x}MgH_3$ (x=0, 0.2, 0.5, 0.8) hydride. In-situ XRD measurements were performed to give a better understanding of the decomposition reactions and phase changes. Figure 3, illustrates the DSC and TGA curves of Li substituted (x=0, 0.2, 0.5, 0.8) samples.
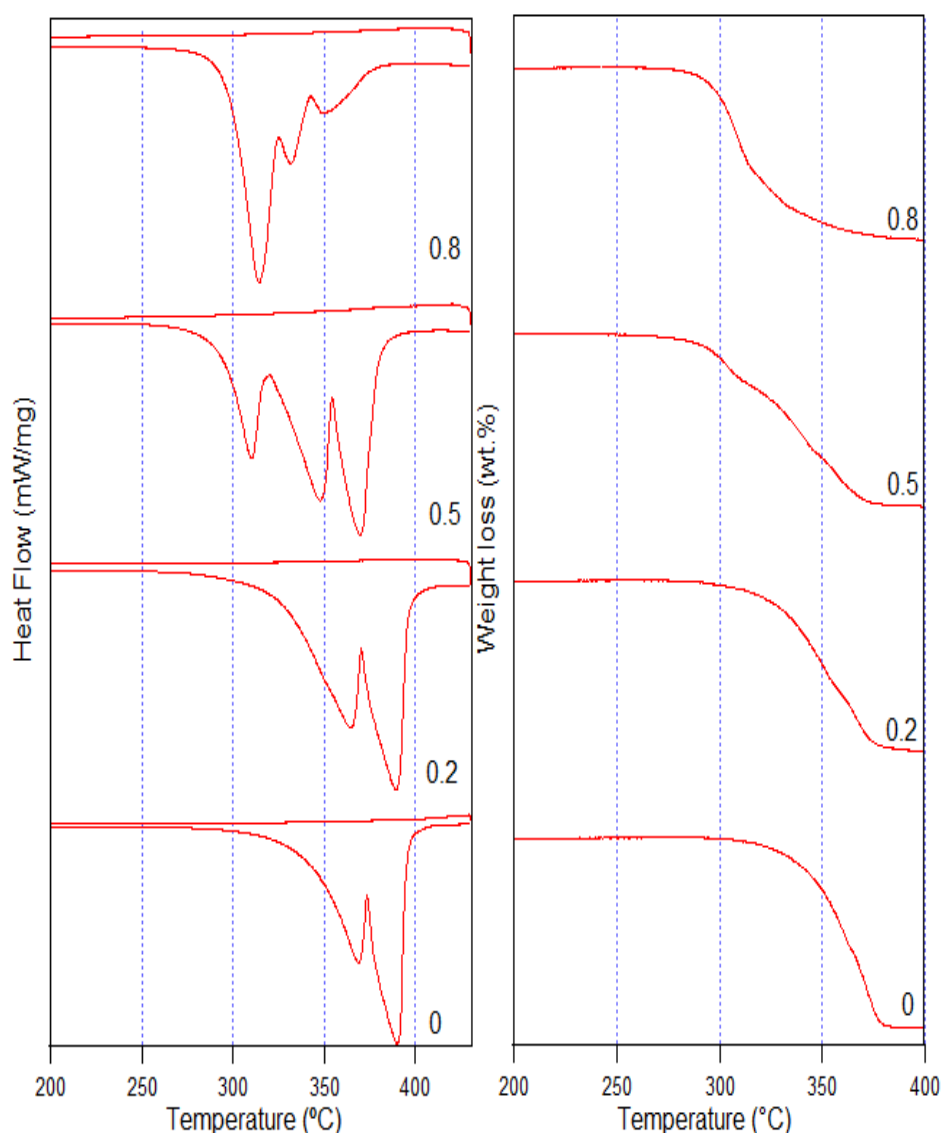

Fig. 3 (left) DSC curves of nominal composition $Li_xNa_{1-x}MgH_3$ hydride system (x=0, 0.2, 0.5 and 0.8) heating rate of 2 °C/min from room temperature to 400 °C and cooling to 30 °C flowing 3 bar Ar at a rate of (100 ml/min) (right) TGA traces of nominal composition $Li_xNa_{1-x}MgH_3$ hydride system (x=0, 0.2, 0.5 and 0.8) heating rate of 2 °C/min from room temperature to 400°C flowing Ar at a rate of (40 ml/min)

3.2.1.1 $Li_xNa_{1-x}MgH_3$ (x=0)

For the sample with Li substitution x=0, two overlapped endothermic reactions can be observed from the DSC peaking at 369 °C and 390 °C, respectively. The first endotherm is attributed to the decomposition of the main $NaMgH_3$ phase into NaH and Mg, whereas, the second curve is related to the NaH decomposition; this corresponded to a total amount of H_2 released of 4.6 wt. % at around 410 °C (TGA).

Figure 4 shows the in-situ XRD of the Li-containing (x=0) sample. At room temperature reflections of $NaMgH_3$ can be observed as one single phase. On heating to 330 °C, peaks of Mg and NaH are observed due to the decomposition of $NaMgH_3$. At 400 °C, more intense diffractions of Mg along with (Mg and Na) oxides were detected. No traces of sodium metal were observed as would have been expected from the decomposition of NaH. However, we assume that Na reflections are present in the sample but become oxidised due to a small leak in the instrument, causing an oxidation layer on the surface of the sample preventing the detection of the Na.
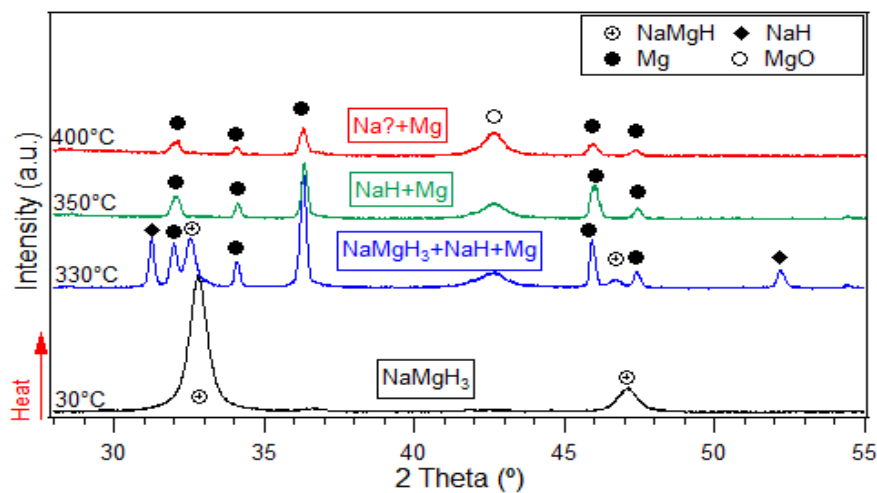

Fig. 4 In-Situ XRD of 5h ball milled LixNa1-xMgH3 (x=0) showing the decomposition reactions of the sample under 3 bar flowing He atmosphere. Measurements were taken from 30°C to 400°C at a rate of 2°C/min.

In order to confirm this assumption, ex-situ XRD was performed on the decomposed sample (Appendix B), where reflections of Na, Mg and some traces of MgO phases were detected.

Decomposition reactions obtained from the measurements performed suggest two steps dehydrogenation for the $Li_xNa_{1-x}MgH_3$ (x=0) as shown in equations 1 and 2. Those results agree with previous reported data [10]:

$$NaMgH_3 \rightarrow NaH+Mg+H_2 \tag{1}$$
$$NaH+Mg+H_2 \rightarrow Na+Mg+3/2H_2 \tag{2}$$
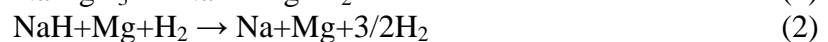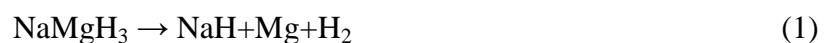
3.2.1.2 $Li_xNa_{1-x}MgH_3$ (x=0.2)

DSC traces of the sample show two endothermic reactions peaking at 360 °C for the $NaMgH_3$ decomposition and 385 °C for the dehydrogenation of NaH. TGA shows a total amount of 5.1 wt. % H_2 is released up to 380 °C. Achieving a peak temperature decrease of around 7 °C in comparison to the sample with Li addition (x=0).

Figure 5 shows the In-situ XRD patterns for the $Li_xNa_{1-x}MgH_3$ hydride with nominal composition (x=0.2). On heating, from room temperature to 300 °C, the only phase detected agrees with the $NaMgH_3$ pattern. At 330 °C, decomposition of $NaMgH_3$ is started, and new phases attributed to NaH, and crystalline Mg starts to form. When heating to 350 °C, reflections of NaH and Mg become more intense, and no traces of $NaMgH_3$ was observed, leading us to the conclusion that decomposition has occurred. At 400 °C, the remaining phases observed correspond to Mg metal and MgO. No evidence of lithium was detected during the decomposition process, although the peaks shift of the main phase (figure 5), suggest that Li ions, when substituted into the system, can cause the lattice and cell contraction of the sample.
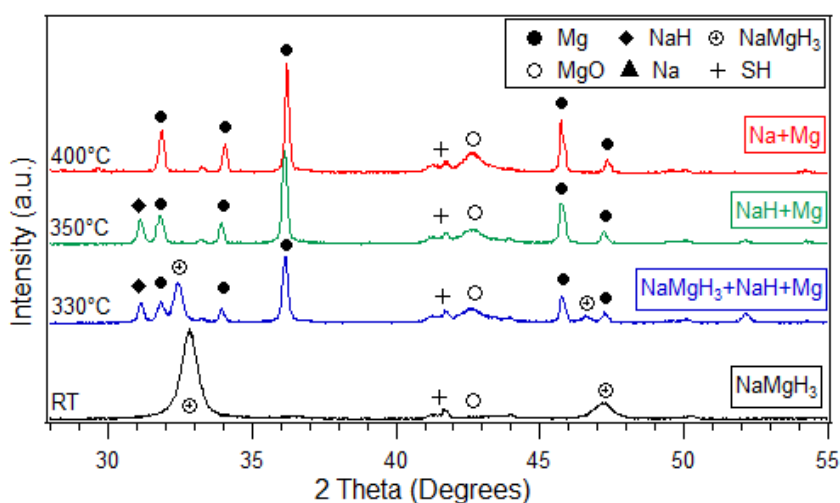

Fig. 5 In-Situ XRD of 5h ball milled LixNa1-xMgH3 (x=0.2) showing the dehydrogenation reactions of the sample under 3 bar flowing He atmosphere. Measurements were taken from RT to 400°C at a rate of 2°C/min.

No traces of crystalline Na were detected as would be expected from the dehydrogenation of NaH phase after 350 °C. Therefore, ex-situ XRD measurements (Appendix B) were carried out on the dehydrogenated sample to investigate this effect. After performing the XRD was elucidated that Na was present in the sample, but due to an oxidation layer on the surface of the sample was not detected by the instrument.

Decomposition reactions of the $Li_{0.2}Na_{0.8}MgH_3$ follow the same two-step dehydrogenation as described above (equations 1 and 2).

3.2.1.3 $Li_xNa_{1-x}MgH_3$ (x=0.5)

For the Li addition x=0.5 DSC traces (figure 3) show three endothermic peaks at 310, 348, 370 °C for the first, second and third decomposition respectively. No exothermic reactions

were observed. The first curve is linked to the MgH_2 decomposition, the decomposition of $NaMgH_3$ phase into NaH and Mg is attributed to the second endotherm, and the final peak is related to the decomposition of NaH into Na along with Mg. The total amount of H_2 released accounts for 5.1 wt. %, from 270 to 380 °C (TGA).

Figure 6 shows the reflections for the In-situ patterns of the $Li_{0.5}Na_{0.5}MgH_3$. At 30 °C, peaks of the $NaMgH_3$ main face, in addition to MgH_2, are detected. On heating up to 250 °C MgH_2 starts to decompose, therefore, small traces of magnesium peaks are perceived at this temperature range. At 330 °C, in addition to the sodium magnesium hydride, a new phase is formed, reflections attributed to NaH are detected corresponding to the decomposition of $NaMgH_3$. MgH_2 patterns are no longer present showing decomposition of the extra magnesium present in the system. Some reflections related to magnesium and lithium oxide are also evident in this temperature range. On heating to 350 °C, sodium magnesium hydride has fully decomposed, since no peaks can be observed. Reflections of magnesium and sodium hydride show increased intensity and patterns for sodium and magnesium and lithium oxides become more evident. At 400 °C, only magnesium phase remains present, in addition to oxide peaks.
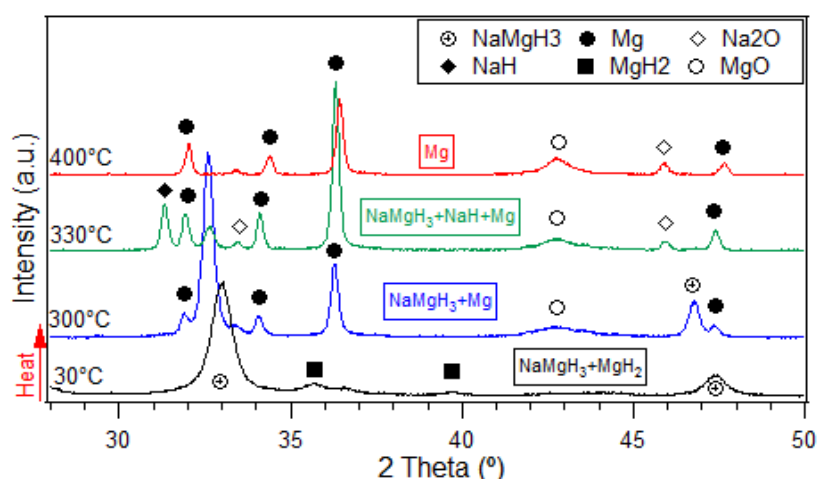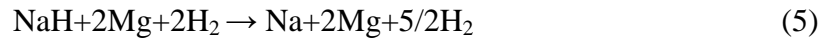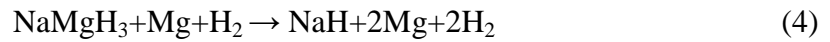

Fig. 6 In-situ XRD of 5h ball milled LixNa1-xMgH3 (x=0.5) showing the dehydrogenation reactions of the sample under 3 bar flowing He atmosphere. Measurements were taken from 30 to 400 °C at a rate of 2 °C/min.

No trace of sodium hydride or sodium metal was detected, while the lithium and magnesium oxide peaks become more intense and sharp. The absence of sodium peaks after sodium hydride decomposition might be explained by the increased intensity of the oxides upon heating. Furthermore, no traces of lithium hydride or metal were evidenced. However, it is inferred they are reacting into the sample due to the patterns shift detected during the heating process.

Ex-situ XRD was performed in the decomposed sample (Appendix B), to investigate the products after decomposition. Peaks related to Mg, Na and MgO were diffracted from the sample.

Decomposition reactions obtained from the measurements performed suggest a three step dehydrogenation for the $Li_{0.5}Na_{0.5}MgH_3$ as shown in equations 3, 4 and 5:

$$NaMgH_3+MgH_2 \rightarrow NaMgH_3+Mg+H_2 \qquad (3)$$

$$NaMgH_3+Mg+H_2 \rightarrow NaH+2Mg+2H_2 \qquad (4)$$

$$NaH+2Mg+2H_2 \rightarrow Na+2Mg+5/2H_2 \qquad (5)$$

3.2.1.4 $Li_xNa_{1-x}MgH_3$ (x=0.8)

DSC and TGA for the $Li_{0.8}Na_{0.2}MgH_3$ exhibit a three stage desorption: the first desorption peak is at 314 °C, the second desorption peak is located at 332 °C, whereas the third desorption peak was centred at 350 °C. A total amount of 5.2 wt. % H_2 was released up to 380 °C.

Figure 7 illustrates the In-situ XRD measurements for the $Li_{0.8}Na_{0.2}MgH_3$ hydride. $NaMgH_2$ and MgH_2 shift to higher 2 theta values on heating up from 30 to 275 °C. Increasing the temperature to 330 °C, the formation of magnesium was observed as a result of the decomposition of MgH_2. Moreover, the intensity of $NaMgH_3$ was reduced and the evidence of NaH reflections was attributed to the decomposition of the $NaMgH_3$. On heating to 350 °C, $NaMgH_3$ reflections were no longer visible. No sodium or lithium peaks can be detected, only magnesium and oxides reflections were observed when heating up to 400 °C. As previously discussed this effect is probably related to the oxidation of the sample during the heating preventing to detect sodium peaks after decomposition of sodium hydride in the case of sodium, as for the lithium it may be assumed that it was present due to the detection of lithium oxide peaks.
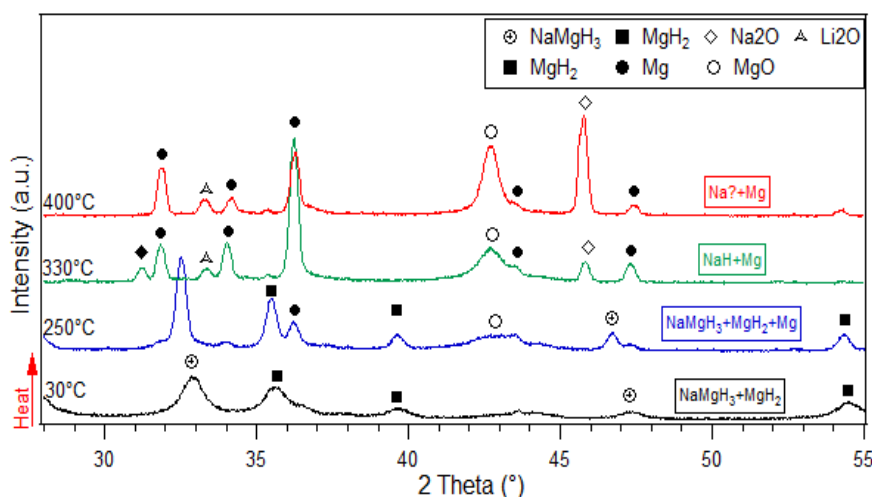

Fig. 7 In-situ XRD of 5h ball milled $Li_xNa_{1-x}MgH_3$ (x=0.8) showing the dehydrogenation reactions of the sample under 3 bar flowing He atmosphere. Measurements were taken from 30 to 400 °C at a rate of 2 °C/min.

The decomposition reactions of the $Li_{0.8}Na_{0.2}MgH_3$ follow the same three step dehydrogenation as described above (equations 3, 4 and 5).

Table 2 summarises the results experimentally gathered in this work for the DSC and TGA measurements.

Table 2
Desorption temperatures and amount of hydrogen release for $Li_xNa_{1-x}MgH_3$

Nominal composition	H2 (wt%)	T ons (°C)	T peak 1,2 & 3 (°C)	T end (°C)
x=0	4.6	275	368 389	386
x=0.2	5.1	258	364 389	397
x=0.5	5.1	254	310 348 369	411
x=0.8	5.2	252	314 330 350	408

3.3 Rehydrogenation (In-Situ XRD)

After dehydrogenation of the Li substitutes hydrides with nominal compositions (x= 0, 0.2, 0.5, 0.8) into Na and Mg metals, samples were heated up to 400 °C under a 10 bar hydrogen atmosphere to investigate if $NaMgH_3$ phase can be reversibly formed.

Figure 8 shows the in-situ XRD measurements of the $Li_xNa_{1-x}MgH_3$ (x=0) sample. On heating from 30 to 100 °C traces of Mg, NaH and (Na and Mg) oxides were detected. On further heating to 200 °C the $NaMgH_3$ phase was detected, showing that the Li substituted (x=0) sample had been successfully rehydrogenated from Na and Mg.

Figure 9 present the in-situ XRD of the $Li_{0.2}Na_{0.8}MgH_3$ hydride. On heating to 200°C the formation of MgH_2 and NaH phases was observed, leading to the formation of $NaMgH_3$ at 300 °C.

Figure 10 illustrates the in-situ XRD patterns of the Li substituted sample (x=0.5) under H_2 atmosphere. Rehydrogenation was accomplished after heating the sample to 300 °C.

Figure 11 shows the in-situ XRD measurements of the $Li_{0.8}Na_{0.2}MgH_3$ hydride. Peaks from hydrogenated magnesium and sodium were detected at 200 °C. Rehydrogenation was observed after heating the sample to 250 °C
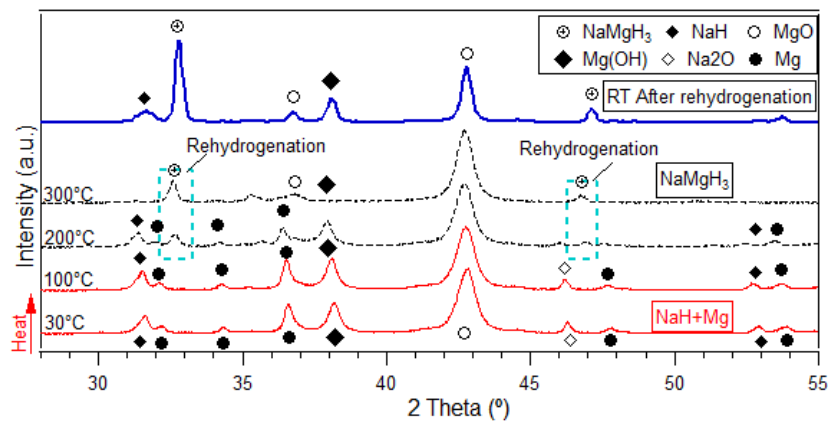
Figure 8 In-situ XRD of the 5 h milled LixNa1-xMgH3 (x=0) rehydrogenated sample under 10 bar H_2 flowing at (100 ml/min) after decomposition. Data was collected isothermally in 50 °C intervals. Dashed (black line) indicates the patterns where rehydrogenation is detected. (Blue thick line on the top of the figure) shows the RT XRD after rehydrogenation process.

Figure 9 In-situ XRD of the 5 h milled LixNa1-xMgH3 (x=0.2) rehydrogenated sample under 10 bar H_2 flowing at (100 ml/min) after decomposition. Data was collected isothermally in 50 °C intervals. Dashed (black line) indicates the patterns where rehydrogenation is detected. (Blue thick line on the top of the figure) shows the RT XRD after rehydrogenation process.
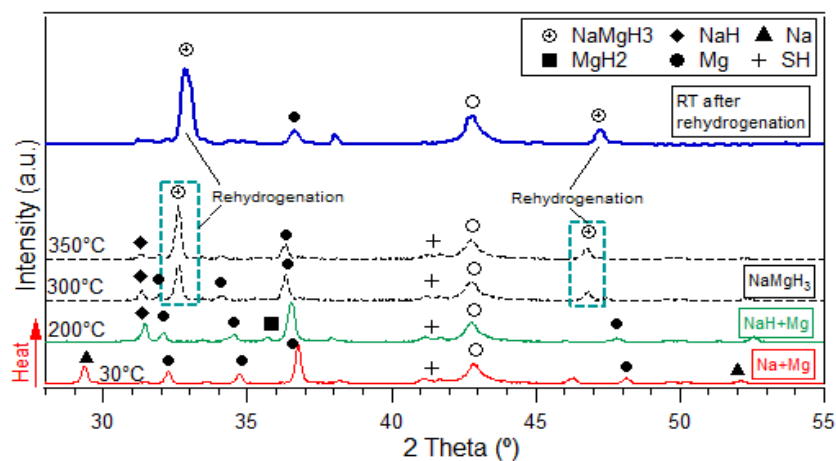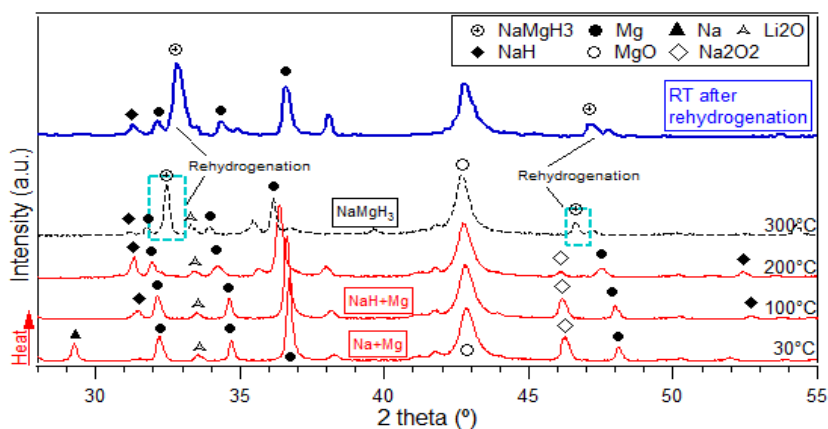

Figure 10 In-situ XRD of the 5 h milled $Li_{0.5}Na_{0.5}MgH_3$ rehydrogenated sample under 10 bar H_2 flowing at (100 ml/min) after decomposition. Data was collected isothermally in 50 °C intervals. Dashed (black line) indicates the patterns where rehydrogenation is detected. (Blue thick line on the top of the figure) shows the RT XRD after rehydrogenation process

Figure 11 In-situ XRD of the 5 h milled $Li_{0.8}Na_{0.2}MgH_3$ rehydrogenated sample under 10 bar H_2 flowing at (100 ml/min) after decomposition. Data was collected isothermally in 50 °C intervals. Dashed (black line) indicates the patterns where rehydrogenation is detected. (Blue thick line on the top of the figure) shows the RT XRD after rehydrogenation process
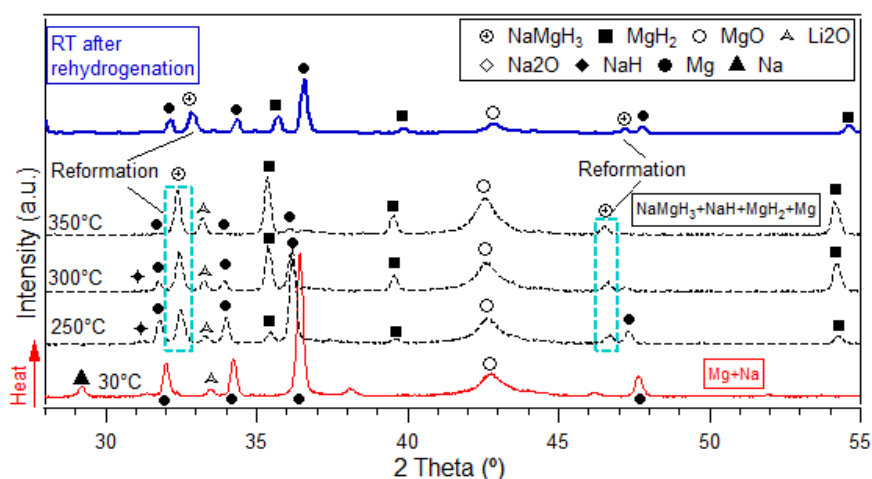
Li substituted samples were reversibly hydrogenated as shown in Figures 8-11 from the elemental Na and Mg phases. These results show that the Li substitution decrease the dehydrogenation temperature from 369 °C for the $Li_xNa_{1-x}MgH_3$ (x=0) sample to 310 °C for the $Li_{0.5}Na_{0.5}MgH_3$ hydride. Furthermore, the amount of released hydrogen is increased from 4.6 wt. % for the $Li_xNa_{1-x}MgH_3$ to 5.2 wt. % for the $Li_{0.8}Na_{0.2}MgH_3$. These results are consistent with predictions based on density functional theory calculation reported by Xiao's group [25], where was found that dehydrogenation enthalpy of perovskite-type $NaMgH_3$ can be lowered by the substitution of Na by Li, hence may result in a favourable modification of the thermodynamics.

4. Conclusions

The $Li_xNa_{1-x}MgH_3$ samples with nominal composition (x=0, 0.2, 0.5, 0.8) were synthesised by mechanical milling under an inert (Ar) atmosphere and pressure: to the best of our knowledge, there are no previous reports of $Li_xNa_{1-x}MgH_3$ preparation under argon alone. Decomposition reactions were investigated experimentally. It was found that both hydrides with Li substitution (x=0 and 0.2) decomposed in two-step reactions, $NaMgH_3 \rightarrow NaH + Mg + H_2$ and $NaH + Mg + H_2 \rightarrow Na + Mg + 3/2H_2$. On the other hand, hydrides containing Li substitution (x=0.5 and 0.8) decomposed in a three-step reactions, $NaMgH_3 + MgH_2 \rightarrow NaMgH_3 + Mg + H_2$, $NaMgH_3 + Mg + H_2 \rightarrow NaH + 2Mg + 2H_2$ and $NaH + 2Mg + 2H_2 \rightarrow Na + 2Mg + 5/2H_2$. Lattice parameters and cell volume of the samples decreased as the Li was introduced into the sample; due to the smaller ionic size of Li^+, up to Li nominal composition (x=0.5), when adding Li (x=0.8) structure of the sample showed an increase in the cell parameters. The highest amount of hydrogen release was achieved with the $Li_{0.8}Na_{0.2}MgH_3$ hydride, where 5.2 wt. % H_2 was released from 252 to 408 °C. Nevertheless, the lowest peak desorption temperature was attained at 308 °C for the $Li_{0.5}Na_{0.5}MgH_3$. Li substituted samples were reversibly formed under 10 bar H_2 at 200 °C for the $Li_xNa_{1-x}MgH_3$ (x=0), 250 °C $Li_{0.8}Na_{0.2}MgH_3$, and at 300 °C for the $Li_xNa_{1-x}MgH_3$ (x=0.2) and $Li_{0.5}Na_{0.5}MgH_3$ from the decomposed Na and Mg metals.

References

[1]   A Bouamrane, JP Laval, J-P Soulie, and JP Bastide, 'Structural Characterization of NaMgH$_3$ F and NaMgH$_3$', *Materials research bulletin,* 35 (2000), 545-49.

[2]   Y. Bouhadda, M. Bououdina, N. Fenineche, and Y. Boudouma, 'Elastic Properties of Perovskite-Type Hydride NaMgH$_3$ for Hydrogen Storage', *International Journal of Hydrogen Energy,* 38 (2013), 1484-89 0360-3199.

[3]   Youcef Bouhadda, Youcef Boudouma, Nour-eddine Fennineche, and Abdelouahab Bentabet, 'Ab Initio Calculations Study of the Electronic, Optical and Thermodynamic Properties of NaMgH$_3$, for Hydrogen Storage', *Journal of Physics and Chemistry of Solids,* 71 (2010), 1264-68.

[4]   Anna-Lisa Chaudhary, Mark Paskevicius, Drew A Sheppard, and Craig E Buckley, 'Thermodynamic Destabilisation of Mgh 2 and NaMgH$_3$ Using Group Iv Elements Si, Ge or Sn', *Journal of Alloys and Compounds,* 623 (2015), 109-16.

[5]   M Fornari, A Subedi, and David J Singh, 'Structure and Dynamics of Perovskite Hydrides a AMgH$_3$ (A= Na, K, Rb) in Relation to the Corresponding Fluorides: A First-Principles Study', *Physical Review B,* 76 (2007), 214118.

[6]   J. Huot, G. Liang, S. Boily, A. Van Neste, and R. Schulz, 'Structural Study and Hydrogen Sorption Kinetics of Ball-Milled Magnesium Hydride', *Journal of Alloys and Compounds,* 293–295 (1999), 495-500.

[7]   K Ikeda, S Kato, Y Shinzato, N Okuda, Y Nakamori, A Kitano, H Yukawa, M Morinaga, and S Orimo, 'Thermodynamical Stability and Electronic Structure of a Perovskite-Type Hydride, NaMgH$_3$', *Journal of Alloys and Compounds,* 446 (2007), 162-65.

[8]   K Ikeda, Y Kogure, Y Nakamori, and S Orimo, 'Formation Region and Hydrogen Storage Abilities of Perovskite-Type Hydrides', *Progress in solid state chemistry,* 35 (2007), 329-37.

[9]   K Ikeda, Y Kogure, Y Nakamori, and S Orimo 'Reversible Hydriding and Dehydriding Reactions of Perovskite-Type Hydride NaMgH$_3$', *Scripta materialia,* 53 (2005), 319-22.

[10]   K Ikeda, Y Nakamori, and S Orimo, 'Formation Ability of the Perovskite-Type Structure in Li$_x$Na$_{1-x}$MgH$_3$ (X= 0, 0.5 and 1.0)', *Acta materialia,* 53 (2005), 3453-57.

[11]   K Komiya, N Morisaku, R Rong, Y Takahashi, Y Shinzato, H Yukawa, and M Morinaga, 'Synthesis and Decomposition of Perovskite-Type Hydrides, MMgH$_3$ (M= Na, K, Rb)', *Journal of Alloys and Compounds,* 453 (2008), 157-60.

[12]   Daixin Li, Tianran Zhang, Siqi Yang, Zhanliang Tao, and Jun Chen, '< I> Ab Initio</I> Investigation of Structures, Electronic and Thermodynamic Properties for Li–Mg–H Ternary System', *Journal of Alloys and Compounds,* 509 (2011), 8228-34.

[13]   R Martínez-Coronado, J Sánchez-Benítez, M Retuerto, MT Fernández-Díaz, and JA Alonso, 'High-Pressure Synthesis of $Na_{1-x}Li_xMgH_3$ Perovskite Hydrides', *Journal of Alloys and Compounds,* 522 (2012), 101-05.

[14]   Office of Energy Efficiency & Renewable. HYDROGEN STORAGE n.d., 'Doe Technical Targets for Onboard Hydrogen Storage for Light-Duty Vehicles'2017) <https://energy.gov/eere/fuelcells/doe-technical-targets-onboard-hydrogen-storage-light-duty-vehicles> [Accessed February, 16 2017].

[15]   S Orimo, and H Fujii, 'Materials Science of Mg-Ni-Based New Hydrides', *Applied Physics A,* 72 (2001), 167-86.

[16]   Daphiny Pottmaier, Eugenio R Pinatel, Jenny G Vitillo, Sebastiano Garroni, Maria Orlova, Maria Dolors Baró, Gavin BM Vaughan, Maximilian Fichtner, Wiebke Lohstroh, and Marcello Baricco, 'Structure and Thermodynamic Properties of the $NaMgH_3$ Perovskite: A Comprehensive Study', *Chemistry of Materials,* 23 (2011), 2317-26.

[17]   Hazel Reardon, Natalia Mazur, and Duncan H Gregory, 'Facile Synthesis of Nanosized Sodium Magnesium Hydride, $NaMgH_3$', *Progress in Natural Science: Materials International,* 23 (2013), 343-50.

[18]   A. H. Reshak, ' $NaMgH_3$' a Perovskite-Type Hydride as Advanced Hydrogen Storage Systems: Electronic Structure Features', *International Journal of Hydrogen Energy,* 40 (2015), 16383-90 0360-3199.

[19]   Ewa Rönnebro, Dag Noréus, Karim Kadir, Alexander Reiser, and Borislav Bogdanovic, 'Investigation of the Perovskite Related Structures of $NaMgH_3$', $NaMgF_3$' and Na_3AlH_6', *Journal of alloys and compounds,* 299 (2000), 101-06.

[20]   Drew A Sheppard, Mark Paskevicius, and Craig E Buckley, 'Thermodynamics of Hydrogen Desorption from $NaMgH_3$' and Its Application as a Solar Heat Storage Medium', *Chemistry of Materials,* 23 (2011), 4298-300.

[21]   Song Tao, Zhong-min Wang, Jia-jun Li, Jian-qiu Deng, Huaiying Zhou, and Qing-rong Yao, 'Improved Dehydriding Properties of $NaMgH_3$' Perovskite Hydride by Addition of Graphitic Carbon Nitride', (2016).

[22]   Song Tao, Zhong-min Wang, Zhen-zhen Wan, Jian-qiu Deng, Huaiying Zhou, and Qingrong Yao, 'Enhancing the Dehydriding Properties of Perovskite-Type $NaMgH_3$' by Introducing Potassium as Dopant', *International Journal of Hydrogen Energy 0360-3199* (2016).

[23]   Zhong-min Wang, Jia-jun Li, Song Tao, Jian-qiu Deng, Huaiying Zhou, and Qingrong Yao, 'Structure, Thermal Analysis and Dehydriding Kinetic Properties of $Na_{1-x}Li_xMgH_3$ Hydrides', *Journal of Alloys and Compounds,* 660 (2016), 402-06.

[24]   Hui Wu, Wei Zhou, Terrence J Udovic, John J Rush, and Taner Yildirim, 'Crystal Chemistry of Perovskite-Type Hydride $NaMgH_3$': Implications for Hydrogen Storage', *Chemistry of Materials,* 20 (2008), 2335-42.

[25]   Xiao-Bing Xiao, Bi-Yu Tang, Sun-Qi Liao, Li-Ming Peng, and Wen-jiang Ding, 'Thermodynamic and Electronic Properties of Quaternary Hydrides $Li_xNa_{1-x}MgH_3$', *Journal of Alloys and Compounds,* 474 (2009), 522-26.

[26]   A. Zaluska, L. Zaluski, and J. O. Ström-Olsen, 'Structure, Catalysis and Atomic Reactions on the Nano-Scale: A Systematic Approach to Metal Hydrides for Hydrogen Storage', *Applied Physics A,* 72 (2001), 157-65.

[27]   L. Zaluski, A. Zaluska, and J. O. Ström-Olsen, 'Nanocrystalline Metal Hydrides', *Journal of Alloys and Compounds,* 253–254 (1997), 70-79.

[28]   BRUKER. EVA Software - The next era in phase analysis n.d. https://www.bruker.com/products/x-ray-diffraction-and-elemental-analysis/x-ray-diffraction/xrd-software/eva/overview.html (accessed October 10, 2016).

[29]   BRUKER. TOPAS Software n.d. https://www.bruker.com/products/x-ray-diffraction-and-elemental-analysis/x-ray-diffraction/xrd-software/topas.html (accessed October 10, 2016).